Supporting Information

Yan et al. 10.1073/pnas.1405198111

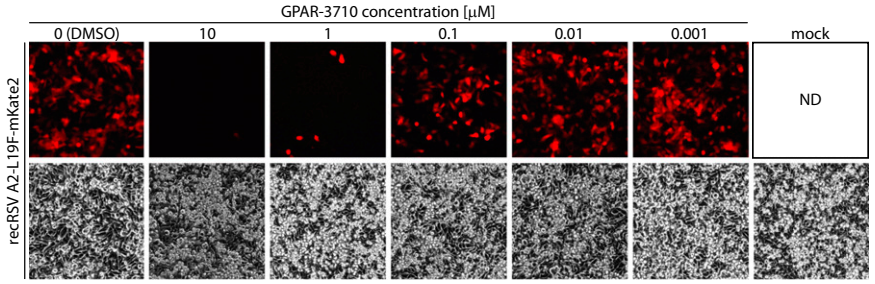

Fig. S1. Inhibition of recRSV A2-L19F-mKate2 by GPAR-3710. Phase contrast and fluorescence microphotographs of cells infected with recRSV A2-L19F-mKate2 in the presence of the specified compound concentrations or vehicle (DMSO) were taken 44 h after infection (p.i.).

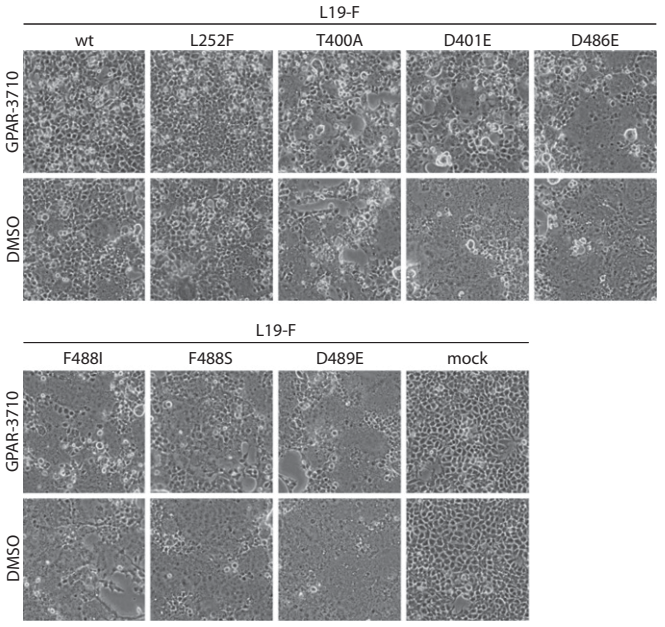

Fig. S2. Resistance testing of RSV F mutants harboring individual escape mutation candidates. Cells were transfected with expression plasmids encoding the specified L19-F mutants and incubated in the presence of 10 μM GPAR-3710 or vehicle (DMSO). Microphotographs were taken 44 h p.i. Mock denotes cells that received vector DNA instead of F expression plasmid.

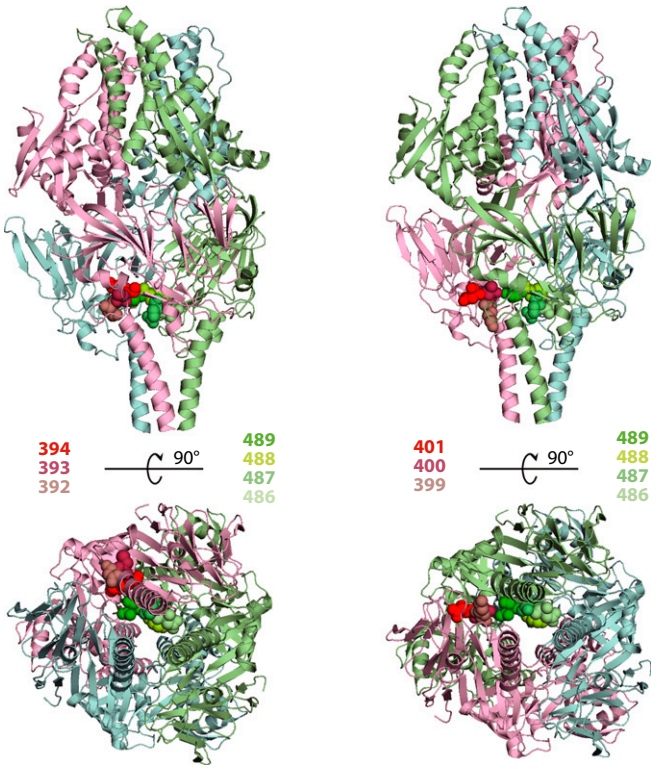

Fig. S3. Ribbon representations of RSV F in the prefusion conformation (PDB ID code 4JHW), colored by monomer. Solid spheres highlight the F 486–489 and F 392–394 (*Left*) or F 399–401 (*Right*) microdomains that were implicated in RSV escape from the diverse panel of entry inhibitors. For clarity of the illustration, the microdomains are highlighted in only one monomer each of the F trimer; note that residues 486-489 of different monomers are highlighted in the left and right panels. Side views and a view from the viral envelope up are shown.

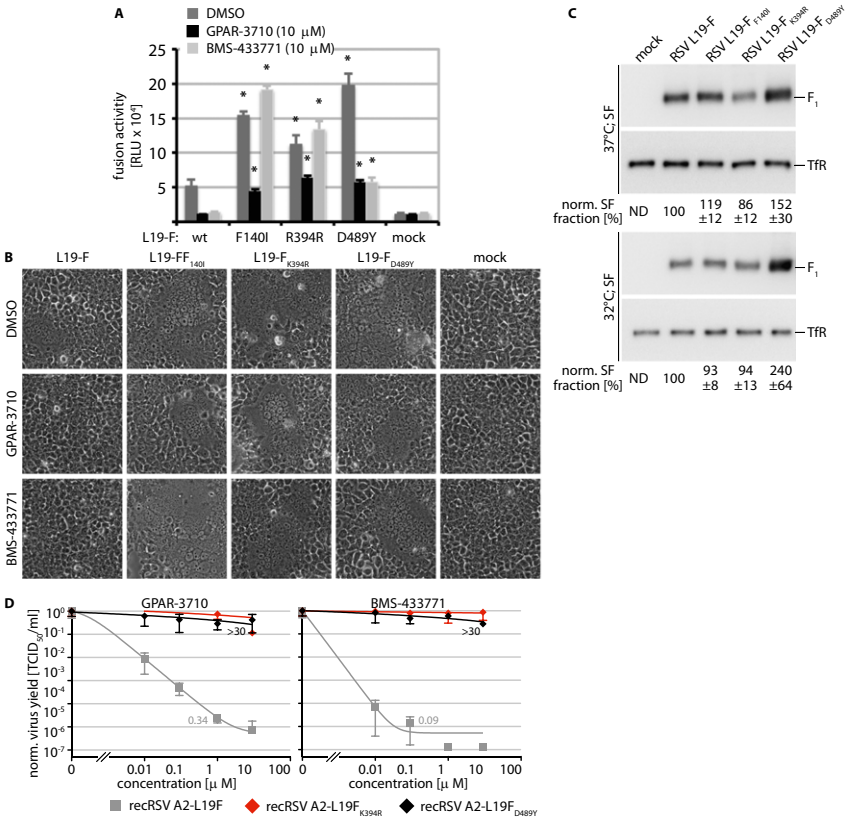

Fig. S4. Effect of escape mutations specifically reported for BMS-433771 on resistance to GPAR-3710 and the RSV F fusion kinetic. (*A*) Resistance quantification using transiently expressed RSV L19-F mutants as outlined for Fig. 3*B*. Values represent means of four experiments ± SD. Datasets were subjected to one-way ANOVA and Bonferroni's multiple comparison posttest; asterisks indicate statistically significant differences of values obtained for individual mutants compared with equally treated, unmodified L19-F ($P < 0.05$). Mock denotes cells transfected with vector DNA instead of F expression plasmid. (*B*) Microphotographs of Hep2 cells expressing unmodified L19-F or L19-F mutants and incubated in the presence of 10 μM GPAR-3710, BMS-433771, or vehicle (DMSO). (*C*) Cell surface expression (SF) of transiently expressed RSV F mutants after incubation of cells at 37 °C or 32 °C. Blots were developed as described in Fig. 5*D*. Numbers denote mean densitometry quantitations of three experiments ± SD, all normalized for TfR and expressed relative to standard L19-F. Mock denotes cells transfected with vector DNA instead of F expression plasmid. (*D*) Dose–response curves after recovery of recombinant RSV recRSV A2-L19FK394R and recRSV A2-L19FD489Y against GPAR-3710 and BMS-433771. Values are mean normalized cell-associated viral titers of three experiments ± SD, EC_{90} concentrations were calculated as in Fig. 1*C* when applicable. Highest concentration assessed, 30 μM.

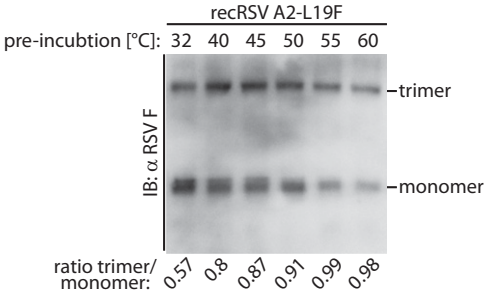

Fig. S5. Fusion core stability assay for RSV F. Purified viral particles were exposed to heat-shock at different temperatures for 10 min, followed by native extraction and fractionation through nonreducing TA-PAGE under mildly denaturing conditions as described in Fig. 6*A*. Immunoblots (IB) were probed with specific antibodies directed against the RSV F protein. The migration pattern of F monomers and fusion core-stabilized trimers is indicated. Numbers below the graph show the relative F trimer:F monomer ratio based on densitometric quantification of signal intensities.

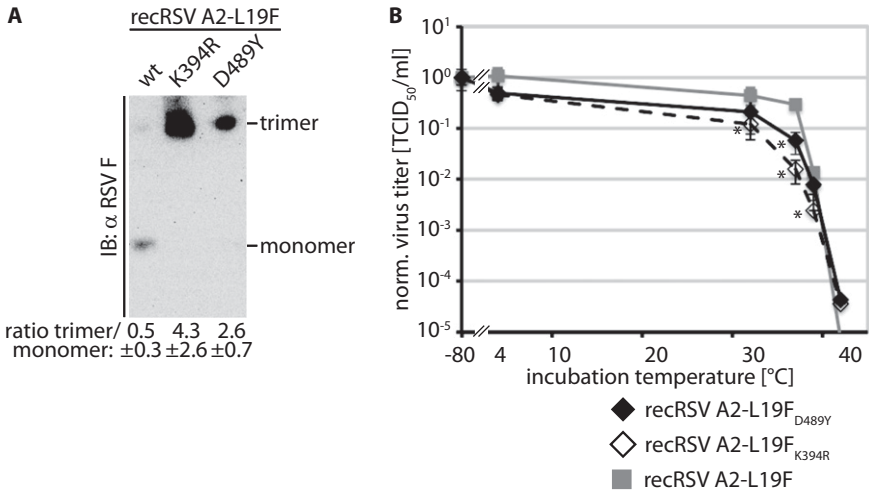

Fig. S6. Stability of RSV recombinants harboring resistance mutations specifically reported for BMS-433771. (*A*) Fusion core assay as described in Fig. 6*A*. The migration pattern of F monomers and fusion core-stabilized trimers is indicated; wt, standard L19F. Numbers below the graph show the mean relative F trimer:F monomer ratio based on densitometric quantification of signal intensities of four experiments ± SD. (*B*) Thermal stability of resistant RSV virions as described in Fig. 6*B*. Values were normalized for aliquots immediately stored at −80 °C for 24 h, and represent means of three experiments ± SD. Asterisks denote statistical analysis of differences between test groups and standard recRSV A2-L19F by one-way ANOVA and Bonferroni's multiple comparison posttest; $*P < 0.05$.

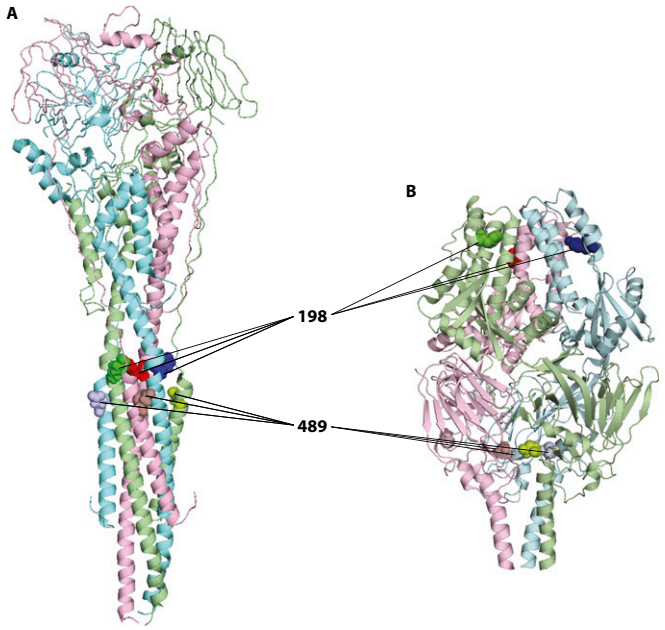

Fig. S7. Ribbon representations of RSV F in the postfusion (*A*; PDB ID code 3RRT) and prefusion (*B*; PDB ID code 4JHW) conformation, colored by monomer. Solid spheres represent for each monomer amino acid side chains at positions 198 and 489, respectively. Side views are shown.

Table S1. Overview of different chemical classes of highly potent RSV entry inhibitors for which resistance hotspots have been mapped

Name	Structure	EC_{50}*	Reported resistance sites†	Source
GPAR-3710		0.13 μM	F_{T400A} F_{D401E} F_{D486E} F_{F488I} F_{F488S} F_{D489E}	This study
TMC353121		0.13 nM	F_{K394R} F_{S398L} F_{D486N}	1
JNJ2408068		2.1 nM	F_{K399I} F_{D486N} F_{E487D}	2
VP-14637		1.4 nM	F_{T400A} F_{F488Y}	2
BMS-433771		10 nM	F_{F140I} F_{V144A} F_{D392G} F_{K394R} F_{D489Y}	3
R170591		2 nM	F_{F488I} F_{F488L} F_{D489Y}	4

*Active concentrations are based on in vitro assays; numbers refer, when available, to the RSV A2 strain.

†Resistance sites in the RSV F protein: Mutations highlighted in red map to the F 400 microdomain; changes in blue affect the F 489 region.

1. Roymans D, et al. (2010) Binding of a potent small-molecule inhibitor of six-helix bundle formation requires interactions with both heptad-repeats of the RSV fusion protein. *Proc Natl Acad Sci USA* 107(1):308–313.
2. Douglas JL, et al. (2005) Small molecules VP-14637 and JNJ-2408068 inhibit respiratory syncytial virus fusion by similar mechanisms. *Antimicrob Agents Chemother* 49(6):2460–2466.
3. Cianci C, et al. (2004) Orally active fusion inhibitor of respiratory syncytial virus. *Antimicrob Agents Chemother* 48(2):413–422.
4. Morton CJ, et al. (2003) Structural characterization of respiratory syncytial virus fusion inhibitor escape mutants: Homology model of the F protein and a syncytium formation assay. *Virology* 311(2):275–288.